Mol. Hum. Reprod. Advance Access published December 8, 2016

Proteolytic degradation of Heat Shock Protein A2 occurs in response to oxidative stress in male germ cells of the mouse

Authors: Elizabeth G. Bromfield[1*], R. John Aitken[1], Eileen A. McLaughlin[1,2], and Brett Nixon[1]

[1]Priority Research Centre for Reproductive Science, School of Environmental and Life Sciences, Discipline of Biological Sciences, University of Newcastle, Callaghan, NSW 2308, Australia

[2] School of Biological Sciences, University of Auckland, Auckland, New Zealand

[*] **To whom correspondence should be addressed:** Elizabeth Bromfield, School of Environmental and Life Sciences, Discipline of Biological Sciences, University of Newcastle, Callaghan, NSW 2308, Australia

Tel: +61 24921 6267

Fax: +61 24921 6308

Email: Elizabeth.bromfield@newcastle.edu.au

Running title: Oxidative stress and HSPA2 degradation in male germ cells

ABSTRACT

Study question: Does oxidative stress compromise the protein expression of heat shock protein A2 (HSPA2) in the developing germ cells of the mouse testis?

Summary answer: Oxidative stress leads to the modification of HSPA2 by the lipid aldehyde 4-hydroxynonenal (4HNE) and initiates its degradation via the ubiquitin-proteasome system.

What is known already: Previous work has revealed a deficiency in HSPA2 protein expression within the spermatozoa of infertile men that have failed fertilization in a clinical setting. While the biological basis of this reduction in HSPA2 remains to be established, we have recently shown that the HSPA2 expressed in the spermatozoa of normozoospermic individuals is highly susceptible to adduction, a form of post-translational modification, by the lipid aldehyde 4HNE which has been causally linked to the degradation of its substrates. This modification of HSPA2 by 4HNE adduction dramatically reduced human sperm-egg interaction *in vitro*. Moreover, studies in a mouse model offer compelling evidence that the co-chaperone BCL2-associated athanogene 6 (BAG6) plays a key role in regulating the stability of HSPA2 in the testis, by preventing its ubiquitination and subsequent proteolytic degradation.

Study design, size, duration: Dose-dependent studies were used to establish a 4HNE-treatment regime for primary culture(s) of male mouse germ cells. The influence of 4HNE on HSPA2 protein stability was subsequently assessed in treated germ cells. Additionally, sperm lysates from infertile patients with established zona pellucida recognition defects were examined for the presence of 4HNE and ubiquitin adducts. A minimum of three biological replicates were performed to test statistical significance.

Participants/materials, setting, methods: Oxidative stress was induced in pachytene spermatocytes and round spermatids isolated from the mouse testis, as well as a GC-2 cell line, using 50 - 200 µM 4HNE or hydrogen peroxide (H_2O_2), and the expression of HSPA2 was monitored via immunocytochemistry and immunoblotting approaches. Using the GC-2 cell line as a model, the ubiquitination and degradation of HSPA2 was assessed using immunoprecipitation techniques and pharmacological inhibition of proteasomal and lysosomal degradation pathways. Finally, the interaction between BAG6 and HSPA2 was examined in response to 4HNE exposure via proximity ligation assays.

Main results and the role of chance: HSPA2 protein levels were significantly reduced compared to controls after 4HNE treatment of round spermatids ($P < 0.01$) and GC-2 cells ($P < 0.001$) but not

pachytene spermatocytes. Using GC-2 cells as a model, HSPA2 was shown to be both adducted by 4HNE and targeted for ubiquitination in response to cellular oxidative stress. Inhibition of the proteasome with MG132 prevented HSPA2 degradation after 4HNE treatment indicating that the degradation of HSPA2 is likely to occur via a proteasomal pathway. Moreover, our assessment of proteasome activity provided evidence that 4HNE treatment can significantly increase the proteasome activity of GC-2 cells ($P < 0.05$ versus control). Finally, 4HNE exposure to GC-2 cells resulted in the dissociation of HSPA2 from its regulatory co-chaperone BAG6, a key-mediator of HSPA2 stability in male germ cells.

Large scale data: Not applicable

Limitations, reasons for caution: While these experiments were performed using a mouse germ cell-model system, our analyses of patient sperm lysate imply that these mechanisms are conserved between mouse and human germ cells.

Wider implications of the findings: This study suggests a causative link between non-enzymatic post-translational modifications and the relative levels of HSPA2 in the spermatozoa of a specific sub-class of infertile males. In doing so, this work enhances our understanding of failed sperm-egg recognition and may assist in the development of targeted antioxidant-based approaches for ameliorating the production of cytotoxic lipid aldehydes in the testis in an attempt to prevent this form of infertility.

Study funding/competing interest(s): This work was supported by the National Health and Medical Research Council of Australia (APP1101953). The authors have no competing interests to declare.

Key words: Sperm, germ cell, ubiquitin, proteasome, degradation, infertility, oxidative stress, chaperone, zona pellucida

INTRODUCTION

Cellular oxidative stress prompts an array of deleterious events in both somatic and germ cells that can lead to cell senescence. Most extensively studied in the male germ line is the effect of potent reactive oxygen species (ROS) on cell function and the devastating consequences of these small molecules on fertility (Aitken et al., 1991; Iwasaki and Gagnon, 1992; Tremellen, 2008; Aitken, 2011). However, emerging research implicating reactive aldehydes, such as 4-hydroxynonenal (4HNE) and acrolein, in cellular damage pathways has uncovered an additional tier of protein regulation in the form of non-enzymatic post-translational modifications (Esterbauer et al., 1991; Uchida and Stadtman, 1992). These aldehyde-induced modifications are particularly pertinent to spermatozoa for two reasons. Firstly, they rely heavily on post-translational modifications to acquire their functional capacity during maturation in both the epididymis and female reproductive tract. Secondly, spermatozoa are laden with ω-6 poly-unsaturated fatty acids that are the key substrates for oxidative attack, yielding high amounts of 4HNE (Jones et al. 1979; Rao et al., 1989; Aitken et al., 2012).

Reactive aldehydes are rapidly produced during the peroxidation of membrane lipids and can modify their target proteins through the formation of stable covalent adducts with the nucleophilic functional groups of cysteine, lysine and histidine residues (Uchida, 2003). This alkylation occurs through both Michael and Schiff base addition reactions and the resulting insertion of a carbonyl group can greatly impact protein function (Esterbauer et al., 1991; Uchida and Stadtman, 1992; Butterfield, 2002; Perluigi *et al*., 2012). Such modifications have the potential to elicit a number of detrimental consequences, such as, protein mis-folding, poor substrate recognition and protein degradation (Perluigi et al., 2012; Uchida and Stadtman, 1992; Carbone et al., 2004).

Though the full extent of the damage that can be elicited within spermatozoa via these aldehyde-induced modifications is yet to be understood, recent studies from our own laboratory have provided evidence that a suite of sperm substrates can be modified by 4HNE (Baker et al., 2015; Aitken et al., 2012; Moazamian et al., 2015). Amongst these targets is heat shock protein A2

(HSPA2), a molecular chaperone that plays fundamental roles in germ cell differentiation (Eddy, 1999), spermiogenesis (Huszar et al., 2006; as reviewed by Scieglinska and Krawczyk, 2015), and in the priming of the sperm surface for oocyte recognition and binding (Redgrove et al., 2012;2013, Bromfield et al., 2015a, reviewed by Nixon et al., 2015). By examining the proteome of spermatozoa from patients exhibiting repeated failure of IVF, we have previously identified severely reduced HSPA2 protein levels as a major feature of their underlying pathophysiology (Redgrove et al., 2012). These results are congruent with independent studies, thus identifying the levels of HSPA2 in mature human spermatozoa as a robust discriminative index of fertilising potential (Ergur et al., 2002; Huszar et al., 2006; Motiei et al., 2013). Accordingly, the modification of HSPA2 brought about by 4HNE adduction was demonstrated to cause a dramatic reduction in human sperm-egg interaction *in vitro*, likely due to the attenuation of HSPA2 chaperoning activity and the resultant failure to correctly position oocyte receptors on the anterior surface of the sperm head (Bromfield et al., 2015a). Importantly, in highlighting the susceptibility of HSPA2 to oxidative insult in mature spermatozoa, these studies have identified a potential mechanism by which HSPA2 function could be compromised in the spermatozoa of patients experiencing repeated IVF failure.

While mildly oxidized proteins have long been considered targets for proteolysis in somatic cells (Grune et al., 1995; Shang et al., 2001; Carbone et al., 2004), the fate of protein substrates modified by 4HNE in the male germ line has not been examined. Interestingly, studies evaluating the innate stability of HSPA2 in mouse germ cells have revealed that this protein is susceptible to proteolytic degradation in the absence of its protective co-chaperone BCL2-associated athanogene 6; BAG6 (Sasaki et al., 2008), a protein that we postulate may provide similar protection to HSPA2 in human germ cells (Bromfield et al., 2015b). Given that causal links have been established between 4HNE adduct formation and protein degradation in other cell types, this study sought to explore the effects of 4HNE on the stability of HSPA2 in the developing germ cells of the mouse testis, as a model for human germ cell development. Additionally, this study aimed to evaluate the use of an immortalized germ cell-derived cell line, the GC-2 cells, to develop a platform for the mechanistic study of HSPA2 stability in the male germ-line under conditions of oxidative stress.

MATERIALS AND METHODS

Ethics approval

All experimental procedures involving animals were conducted with the approval of the University of Newcastle's Animal Care and Ethics Committee (ACEC) (approval number A-2013–322). Inbred Swiss mice were obtained from a breeding colony held at the institutes' central animal house and maintained according to the recommendations prescribed by the ACEC. Mice were housed under a controlled lighting regime (16L:8D) at 21–22 °C and supplied with food and water ad libitum. Prior to dissection, animals were euthanized via CO_2 inhalation. All other experiments were conducted with human semen samples obtained with informed written consent from a panel of IVF patients enrolled in ART programmes with IVFAustralia (Greenwich, NSW, Australia). Volunteer involvement and all experimental procedures were performed in strict accordance with institutional ethics approvals granted by the University of Newcastle Human Research and Ethics Committee (Approval No. H-2013-0319) and the IVFAustralia Ethics Committee with written consent obtained from all participants. All sperm samples were subjected to analyses in accordance with the World Health Organization guidelines (WHO, 2010), and patients were selected on the basis of failed IVF associated with poor zona pellucida adherence following overnight incubation with a minimum of five oocytes.

Reagents

Unless specified, chemical reagents were obtained from Sigma-Aldrich (St. Louis, MO, USA) and were of research grade. Cell culture reagents were purchased from Sigma or ThermoFisher Scientific (Waltham, MA, USA). The following primary antibodies were purchased to characterize proteins of interest: rabbit polyclonal anti-HSPA2 (Sigma-Aldrich; Cat # SAB1405970); mouse monoclonal anti-ubiquitin (Abcam, Cambridge, UK; Cat # ab7254); rabbit monoclonal anti-ubiquitin (linkage-specific

k48) (Abcam; Cat # ab140601), rabbit polyclonal anti-4HNE (Jomar Bioscience, Kensington, VIC, Australia; Cat # HNE11-S), mouse monoclonal anti-BAG6 (Santa Cruz Biotechnology, Dallas, TX, USA; Cat # sc-365928) and rabbit polyclonal anti-Fibrillarin (Abcam; Cat # ab5821). The aldehyde purchased for these studies was 4HNE (Cayman Chemicals, Ann Arbor, MI, USA). Albumin and 3-[(3-cholamidopropyl)dimethylammonio]-1-propanesulfonate (CHAPS) were obtained from Research Organics (Cleveland, OH, USA) and DMEM was purchased from Life Technologies (Mulgrave, VIC, Australia). Tris was purchased from ICN Biochemicals (Castle Hill, NSW, Australia), nitrocellulose was from GE Healthcare (Buckinghamshire, UK), Mowiol 4-88 was from Calbiochem (La Jolla, CA, USA), and paraformaldehyde was supplied by ProSciTech (Thuringowa, QLD, Australia). For immunoprecipitation studies Protein G beads and a 3,3′-dithiobis[sulfosuccinimidylpropionate] (DTSSP) cross-linker were purchased from ThermoFisher Scientific. Appropriate horse-radish peroxidase (HRP)-conjugated secondary antibodies were obtained from Santa Cruz Biotechnology and Sigma-Aldrich.

Germ cell isolation

Enriched populations of spermatocytes and spermatids were recovered from dissected adult mouse testes using density sedimentation at unit gravity as described previously (Baleato et al., 2005). Briefly, testes were disassociated and tubules were sequentially digested with 0.5 mg/ml collagenase/DMEM and 0.5% v/v trypsin/EDTA to remove extra-tubular contents and interstitial cells. The remaining isolated cells were loaded onto a 2 – 4% w/v bovine serum albumin (BSA)/DMEM gradient to separate male germ cell types according to density. This method results in the isolation of germ cells with very little to no somatic cell contamination, as extra-tubular cells are digested and removed prior to density sedimentation (Nixon et al., 2014; Baleato et al., 2005). These isolations achieved ~81% purity for pachytene spermatocytes (PS) and ~89% purity for round spermatids (RS) with remaining contamination limited to the presence of some lepotene, zygotene and diplotene spermatocytes for ‘PS’ preparations and late/elongating spermatids for ‘RS’ preparations (Nixon et al., 2014; Katen et al., 2016).

191 *Cell culture*

192 The murine spermatogenic cell line GC-2 spd (ts) (hereafter referred to as GC-2; American Type
193 Culture Collection, Manassas, VA, USA) was cultured in DMEM supplemented with 100 mM sodium
194 pyruvate, 200 mM L-glutamate, 100 U/ml penicillin, 10 mg/ml streptomycin, and 5% fetal calf serum
195 and grown to confluence at 37 °C under 5% CO_2 with medium renewed every 2–3 days. Cells were
196 harvested for all assays using trypsin/EDTA, re-suspended in fresh DMEM and treated in solution.

197 *4HNE treatment and viability assessment*

198 Oxidative stress was induced in populations of isolated spermatocytes, spermatids and GC-2 cells
199 through treatments with 4HNE at concentrations of 50, 100 and 200 μM, or with hydrogen peroxide
200 (H_2O_2) at concentrations of 50 and 200 μM, based on previous studies (Bromfield et al., 2015a).
201 4HNE and H_2O_2 were chosen to induce oxidative stress based on their efficacy established in previous
202 studies (Aitken et al., 2012; Bromfield et al., 2015a; Baker et al., 2015). Cells were re-suspended in 1
203 ml sterile DMEM, supplemented with 100 μM sodium pyruvate, 200 μM L-glutamate, 100 U/ml
204 penicillin, 10 μg/ml streptomycin, and 5% v/v fetal bovine serum. Upon addition of 4HNE (50, 100
205 and 200 μM) or H_2O_2, cells were incubated for a period of 3 h at 37 °C. After treatment, cell viability
206 was assessed using an eosin vitality stain as previously described (Aitken et al., 2012). Based on
207 viability scores across replicate experiments, a 4HNE concentration of 50 μM and duration of 3 h was
208 selected for the treatment of both spermatocytes and spermatids. For GC-2 cells, concentrations of 50
209 μM and 200 μM 4HNE were used throughout the study as specified and cells were exposed to 4HNE
210 for 3 h.

211 *Sodium dodecyl sulphate (SDS) polyacrylamide gel electrophoresis and immunoblotting*

212 Following treatment with 4HNE, spermatids, spermatocytes and GC-2 cells were washed once in
213 DMEM, pelleted via centrifugation for 5 min at 500 x *g* and resuspended for SDS-based protein
214 extraction, as previously described (Reid et al., 2012). Protein extracts were then boiled in the
215 presence of NuPAGE LDS sample buffer (Invitrogen) containing 8% β-Mercaptoethanol, subjected to
216 SDS polyacrylamide gel electrophoresis (SDS–PAGE) using 4–12% Bis–Tris gels (ThermoFisher

Scientific) and then electro-transferred to nitrocellulose membranes using conventional Western blotting techniques (Towbin et al., 1979). To detect proteins of interest, membranes were blocked in 3% BSA in Tris-buffered saline supplemented with 0.1% Tween-20 (TBST, pH 7.4) then probed with either anti-HSPA2 diluted 1:1000, anti-UBI-1 diluted 1:500; anti-UBI-k48 diluted 1:500; or anti-4HNE diluted 1:1000 in TBST supplemented with 1% BSA under constant rotation overnight at 4 °C. Membranes were washed in TBST (3 × 10 min at room temperature) and appropriate secondary antibodies were applied for 1 h at room temperature under constant rotation. After a further three washes, labelled proteins were visualized using an enhanced chemiluminescence detection kit (ECL plus, Amersham Bioscience, UK) according to the manufacturer's instructions. After development, all Western blots were stripped prior to being re-incubated in anti-α-tubulin antibodies and its corresponding secondary antibody, as above, to determine relative loading. Band density was quantified over three replicate blots using Image J software (version 1.48v; National Institute of Health, Bethesda, MD, USA)) and expressed relative to α-tubulin labelling intensity.

Immunocytochemistry

Following treatment, cells were fixed in 4% paraformaldehyde, washed 3× with 0.05 M glycine in phosphate-buffered saline (PBS) at room temperature and then pipetted in 50 µl aliquots onto poly-L-lysine-coated glass coverslips and allowed to settle for > 3 h. Non-adherent cells were removed with one wash of PBS then cells were permeabilized with 0.2% Triton X-100 and placed in a humid chamber for blocking with 3% BSA/PBS for 1 h. Coverslips were then washed in PBS and incubated in anti-ubiquitin or anti-HSPA2 antibodies diluted 1:500 or 1:1000, respectively, overnight at 4°C. Following this, coverslips were washed (3 × 5 min) in PBS before applying appropriate secondary antibodies diluted 1:100 with 1% BSA/PBS for 1 h at room temperature. Coverslips were washed in PBS (3 × 5 min) before mounting in 10% mowiol 4-88 (Calbiochem) with 30% glycerol in 0.2 M Tris (pH 8.5) and 2.5% 1,4-diazabicyclo-(2.2.2)-octane (DABCO). Cell labelling was examined with a Zeiss LSM510 laser scanning confocal microscope (Carl Zeiss Pty, Sydney, Australia). Fluorescence intensity analysis was performed by recording the fluorescence of ~ 50 isolated germ cells over three replicates using ImageJ software.

244 *Immunoprecipitation*

245 Untreated and 50 μM H_2O_2 treated GC-2 cells were lysed at 4°C for 2 h in lysis buffer consisting of
246 10 mM CHAPS, 10 mM HEPES, 137 mM NaCl and 10% glycerol with the addition of protease
247 inhibitors (Roche). The cell lysates were then added to 50 μl aliquots of washed protein G Dynabeads
248 and incubated under rotation to preclear at 4°C for 1 h. Anti-HSPA2 antibody, 10 μg in 200 μl of
249 PBS, was conjugated to fresh aliquots of washed Dynabeads by incubation for 2 h at 4°C under
250 rotation. Following antibody binding, the cross-linking reagent, 3,3'-
251 dithiobis[sulfosuccinimidylpropionate] (DTSSP), was added at a final concentration of 2 mM and
252 crosslinking was performed at room temperature for 30 min after which 20 mM Tris was added to
253 each tube for an additional 15 min at room temperature to quench the reaction. Immunoprecipitation
254 was then performed by adding 1 ml pre-cleared lysate to HSPA2 antibody bound beads and
255 incubating under rotation overnight at 4°C. After incubation, supernatants were transferred to clean
256 tubes and washed (3×) in 200 μl of PBS at room temperature. Target antigen was eluted from the
257 beads by boiling in the presence of SDS loading buffer containing 8% β-Mercaptoethanol with the
258 same elution step performed on preclear beads. These solutions were loaded onto a NuSep 4-20%
259 Tris-glycine gel for analysis via SDS-PAGE. In addition, bead only and antibody only controls were
260 prepared by loading 10 μl of protein-G bead slurry and 5 μl of anti-HSPA2 in the presence of SDS-
261 loading buffer into appropriate gel lanes. Gels were loaded in triplicate, resolved at 150 V for ~1 h
262 and prepared for immunoblotting with anti-UBI-k48 and anti-4HNE antibodies.

263 *Proteasome activity assay and inhibitor studies*

264 To assess proteasome activity in response to 4HNE treatment, spermatocytes, spermatids and GC-2
265 cells were washed twice in DMEM and cell concentration was adjusted to ensure equal cell numbers
266 across each population. All cell suspensions were lysed in 100 μl of nonidetP40 (NP40) protein
267 extraction buffer composed of; 150 mM sodium chloride, 50 mM Tris and 0.5% NP40, for 30 min
268 under constant rotation at 4 °C. After centrifugation at 16300 x g for 15 min supernatants were
269 transferred to a clean tube and then assessed for proteasome activity using a commercial proteasome

assay kit that utilizes an 7-amino-4-methylcoumarin (AMC)- tagged peptide substrate, which releases highly fluorescent AMC in the presence of proteolytic activity (Abcam, ab107921). Briefly, 25 µl of each sample was loaded into a 96 well plate in duplicate, alongside a Jurkat cell lysate positive control (supplied) and AMC protein standards. To one well of each sample and control, 1 µl of proteasome inhibitor MG132 was added to differentiate proteasome activity from other protease activity that may be present in the samples.

Plates were incubated for 30 min and then analysed on a BMG Fluostar Optima plate reader (BMG Labtech, Mornington, VIC, Australia) at an excitation/emission = 350/440 nm. Following a further 30 min incubation at 37 °C, plates were analysed a second time to allow the change in relative fluorescence units (ΔRFU) to be calculated for each sample. Data were analysed following the manufacturers' instructions and proteasome activity was calculated such that one unit of proteasome activity is equivalent to the amount of proteasome activity that generates 1.0 nmol of AMC per minute at 37°C.

To further investigate the role of the proteasome, GC-2 cells were treated with either a proteasome inhibitor MG132 (10µM) or a lysosome inhibitor (chloroquine: 100µM) for the duration of 4HNE exposure and then cells were lysed and prepared for immunoblotting experiments with anti-HSPA2 antibodies (as above).

Proximity ligation assay

Duolink *in situ* primary ligation assays (PLAs) were conducted in accordance with the manufacturers' instructions on fixed GC-2 cells adhered to poly-L-lysine coated coverslips (Sigma-Aldrich). Briefly, samples were blocked in Duolink blocking solution and then incubated with primary antibodies (anti-BAG6, anti-HSPA2 and anti-tubulin) overnight at 4°C. Oligonucleotide conjugated secondary antibodies (PLA probes) were then applied for 1 h at 37°C and ligation of the PLA probes was performed and the signal amplified. The fluorescent signal generated when molecules are in close association (< 40 nm) was visualized using fluorescence microscopy and pixel intensity scores were generated using Image J image analysis software (Version 1.48v; NIH, USA) for untreated and 4HNE

296 treated GC-2 cells. The specificity of the PLA reaction was ensured by performing proximity ligation
297 with antibodies to the target antigens combined with anti-tubulin antibodies with which they should
298 not interact, as described previously (Bromfield et al., 2016).

299 *Statistics*

300 All experiments were replicated at least 3 × with independent samples and data are expressed as mean
301 values ± S.E. Statistical analysis was performed using a two-tailed, unpaired Student's t test using
302 Microsoft Excel (Version 14.0.7143.5000; Microsoft Corp., Redmond, WA, USA) Differences were
303 considered significant for $p < 0.05$.

304

305

306 **RESULTS**

307 *The effect of 4HNE treatment on HSPA2 expression in developing mouse germ cells*

308 Initial experiments focused on titration of exogenous 4HNE exposure to identify optimal conditions
309 that were capable of eliciting a state of oxidative stress without significantly compromising the
310 cellular viability of PS, RS, or GC-2 cells (i.e. maintenance of a minimal threshold above 70%
311 viability in each population of cells). On the basis of data from previous studies of mature
312 spermatozoa, we adopted a 4HNE exposure period of 3 h with concentrations of the aldehyde ranging
313 from 50 - 200 µM (Aitken et al., 2012, Moazamian et al., 2015; Baker et al., 2015; Bromfield et al.,
314 2015a). As expected, the viability of all mouse germ cells declined in a dose-dependent manner
315 following 4HNE exposure. Notably however, primary cultures of PS and RS were deemed more
316 sensitive to 4HNE insult than the GC-2 cell line, with 200 µM 4HNE reducing the number of viable
317 cells to 52%, 63% and 70% in the target populations of PS, RS and GC-2 cells, respectively. From
318 these observations, a 3 h treatment regime was selected comprising 200 µM 4HNE exposure for GC-2
319 cells and a lower concentration of 50 µM 4HNE for both PS and RS (Supplementary Figure 1A).

Following exposure to these 4HNE treatment conditions, PS, RS and GC-2 cells were evaluated for their levels of HSPA2 protein expression relative to that of untreated cells incubated for an equivalent period in media alone (Figure 1). Immunoblotting of cell lysates with anti-HSPA2 antibodies revealed that HSPA2 protein expression was not significantly affected in lysates recovered from 4HNE treated PS (Figure 1A). Similarly, elevating the dose of 4HNE to 200 μM (equivalent to that used for GC-2 cells) did not yield any detectable changes in HSPA2 levels in the pachytene spermatocytes (Supplementary Figure 1B). However, in marked contrast, a highly significant reduction in HSPA2 expression relative to anti-tubulin loading controls for both RS (Figure 1B) and GC-2 cells (Figure 1C) was observed. Of these two cell types, HSPA2 expression proved the most sensitive within the GC-2 cells, with the protein being barely detectable in the lysates isolated from 4HNE treated GC-2 cells (Figure 1C).

Equivalent data were also obtained in immunocytochemistry experiments whereby HSPA2 protein expression was detected throughout the cytosol and extending into the nucleus of all untreated germ cells examined. In the case of PS, neither the intensity nor the localization of HSPA2 labelling appeared to be impacted by 4HNE treatment (Figure 2A). However, HSPA2 labelling was significantly reduced in both 4HNE treated RS (Figure 2B; $P < 0.01$) and GC-2 cells (Figure 2C; $P < 0.01$), to the point where it was virtually undetectable in the latter cells.

As HSPA2 has proven to be vulnerable to ubiquitin-dependent degradation in a previous study characterizing *Bat3* (*Bag6*) deficiency in the male germline (Sasaki et al., 2008), we next evaluated the expression of ubiquitin in PS, RS and GC-2 cells in response to 4HNE treatment. This experiment simultaneously permitted the assessment of cellular ubiquitin levels in response to 4HNE exposure. Immunocytochemistry with anti-UBI-1 revealed the presence of ubiquitin at basal levels in both the cytoplasmic and nuclear compartments of untreated PS, RS and GC-2 cells. Upon 4HNE treatment, a global increase in UBI-1 fluorescence was observed in RS and GC-2 cells but surprisingly this also occurred in PS despite their apparent resilience to HSPA2 loss (Figure 2). Although no overt re-localization of ubiquitin was detected in each cell population, the nuclear expression of ubiquitin did display a modest increase in RS after 4HNE exposure (Figure 2B).

This series of experiments uncovered a stage-dependent disparity in the vulnerability of HSPA2 to oxidative insult in developing germ cells, with the expression of the protein proving particularly susceptible to 4HNE in RS. Additionally, under our experimental conditions the GC-2 cell line more closely reflected the behavior of the isolated RS population rather than that of the PS population. This cell line afforded the additional advantages that they were more resilient to 4HNE treatment, and could be more readily cultured *in vitro* than PS and RS. Thus, for the purpose of this study, GC-2 cells were selected as a model for RS and used to gain further mechanistic insight into the loss of HSPA2 during germ cell development.

Exploring a link between 4HNE adduction and ubiquitination of HSPA2 in the GC-2 cell line

In previous studies focusing on mature human spermatozoa, we have provided evidence that HSPA2 is selectively targeted for 4HNE adduction under conditions of oxidative stress (Bromfield et al., 2015a). While this adduction did not result in a loss of HSPA2 expression in mature sperm cells, we predict that this modification may have more deleterious effects on HSPA2 stability in developing germ cells. To determine whether 4HNE treatment can result in the ubiquitination of HSPA2, GC-2 cells were treated with either 50 µM or 200 µM 4HNE and ubiquitination was examined using an anti-UBI-k48 antibody. This antibody was selected for use as the K48 polyubiquitin chains are preferentially involved in signaling target proteins for proteasomal degradation (Mallette and Richard, 2012). Immunoblotting with anti-UBI-k48 revealed numerous constitutively ubiquitinated protein substrates in untreated GC-2 cells (Figure 3A) However, treatment with 50 µM 4HNE augmented this ubiquitin profile resulting in the presence of a distinct ubiquitin-substrate band of approximately 72 kDa. Moreover, increasing the concentration of 4HNE to 200 µM (a concentration at which HSPA2 expression is virtually ablated in these cells, Figures 1C and 2C) resulted in the loss of this band from the ubiquitinated protein profile (Figure 3A). Incubation of corresponding membranes in anti-HSPA2 antibodies revealed the co-migration of this ubiquitinated substrate with HSPA2 at 72 kDa and, as predicted, 50 µM 4HNE induced a modest reduction in HSPA2 expression while 200 µM treatments resulted in an absence of the 72 kDa HSPA2 band (Figure 3B). Interestingly, with the exception of a prominent ubiquitinated band of ~100 kDa that was lost upon exposure of GC-2 cells to either 50 or

200 µM 4HNE, these treatments had limited additional impact on the profile of ubiquitinated proteins detected within GC-2 cell lysates (Figure 3A).

To further validate the adduction and ubiquitination of HSPA2 under conditions of oxidative stress, the protein was immunoprecipitated from GC-2 cell lysates recovered from untreated and H_2O_2 (50 µM) treated cells. In this instance, oxidative stress was induced with H_2O_2 in order to enable an accurate study of 4HNE adduction without the confounding factor of the exogenous 4HNE used to induce oxidative stress. As a prelude to this study we first verified the ability of H_2O_2 (50 and 200 µM) to elicit a reduction in HSPA2 protein expression in GC-2 cells comparable to that observed with 4HNE (Supplementary Figure 1C). Following immunoprecipitation, eluted proteins were probed with anti-HSPA2 (to confirm the efficacy of the method; Figure 4A), anti-4HNE (to identify protein adducts; Figure 4B) and anti-UBI-k48 antibodies to confirm ubiquitination of HSPA2 (Figure 4C). In both the treated and untreated eluates, the HSPA2 protein was effectively isolated as indicated by the predominant band at ~72kDa. As predicted, substantially more HSPA2 was detected in the immunoprecipitated protein from untreated GC-2 cells (Figure 4A). Despite this, probing corresponding blots with anti-UBI-k48 (Figure 4B) and anti-4HNE (Figure 4C) revealed the presence of these molecules at ~72kDa uniquely within the H_2O_2 treated GC-2 cell elution lanes. Importantly, the specificity of this immunoprecipitation was confirmed through use of antibody-only and bead-only controls, as well as a 'precleared' control, each of which failed to show any labelling of the 72 kDa band corresponding to HSPA2.

The influence of 4HNE on HSPA2 proteolysis

While the ubiquitination of HSPA2 implies that this protein may be subject to proteolysis in response to oxidative stress, we sought to explicitly confirm this using the proteasome inhibitor MG132. When GC-2 cells were treated with 4HNE in the presence of MG132, the HSPA2 protein was clearly detected by immunoblotting at a level that appeared indistinguishable from that of untreated cells (Figure 5A). This finding suggests that the degradation of HSPA2 could indeed be prevented by attenuating proteasome activity. Moreover, the use of a lysosomal inhibitor, chloroquine, at a 100 µM

concentration previously reported to block the lysosomal degradative pathway (Dunmore et al., 2013; Koh et al., 2005), did not prevent the loss of HSPA2 expression (Figure 5B), thus providing further evidence that the degradation of HSPA2 is likely to proceed via a proteolytic pathway. Finally, to examine whether oxidative stress modulates global proteasome activity in GC-2 cells, a proteasome activity assay was employed. This assay revealed a 1.7-fold increase in proteasome activity in cells exposed to 4HNE when compared to their untreated counterparts (Figure 5C), suggesting that 4HNE may be capable of influencing proteasome activity in GC-2 cells.

To gain further mechanistic insight into the loss of HSPA2 from oxidatively stressed GC-2 cells, we turned our attention to its protective co-chaperone, BAG6, which has formerly been implicated in the regulation of HSPA2 stability in mouse testicular germ cells (Sasaki et al., 2008). Our analysis of BAG6 expression via immunoblotting and immunocytochemistry confirmed the presence of the protein in both 4HNE treated and untreated GC-2 cell populations with no significant difference in band density detected (Figure 6A). However, in 4HNE treated cells a shift in the localization of BAG6 was detectable with >70% of 4HNE treated GC-2 cells displaying BAG6 fluorescence primarily around the periphery of the cell rather than the uniform expression throughout the cytosol that was observed in untreated GC-2 cells (Figure 6B). Furthermore, in a complimentary experiment untreated and 4HNE-treated GC-2 cells were separated into their nuclear and cytoplasmic compartments and prepared for Western blotting alongside an accompanying whole cell lysate. The efficacy of this subcellular fractionation was confirmed through immunoblotting with anti-tubulin and anti-Fibrillarin antibodies to demonstrate an enrichment of cytoplasmic and nuclear components, respectively. Importantly, probing of corresponding Western blots with anti-BAG6 revealed a modest reduction in BAG6 protein expression in the nuclear fraction of 4HNE-treated GC-2 cells and a corresponding subtle increase in BAG6 present in the cytoplasmic fraction (Supplementary Figure 2). Given this apparent re-localization, we next verified whether BAG6 and HSPA2 could form a stable interaction in GC-2 cells by employing a PLA, similar to that we have previously used to establish a relationship between BAG6 and HSPA2 in human spermatozoa (Bromfield et al., 2015a). This assay confirmed the association of BAG6 and HSPA2 in untreated GC-2 cells (Figure 6C). Conversely, GC-

2 cells that had been treated with 4HNE displayed little PLA signal suggesting that the two proteins examined no longer reside in close enough proximity to form a stable interaction (Figure 6C). The specificity of the proximity ligation was verified by performing the assay with anti-BAG6 and anti-tubulin antibodies as previously described (Supplementary Figure 2A). To further support these data, immunoprecipitation experiments were performed using HSPA2 as bait to assess the interaction between BAG6 and HSPA2 in response to 4HNE treatment (Figure 6D). Probing immunoprecipitation blots with anti-BAG6 revealed a concomitant reduction in BAG6 in the eluate of GC-2 cells exposed to 4HNE. Importantly, the efficacy of the immunoprecipitation was confirmed through the interrogation of corresponding immunoblots with anti-HSPA2 revealing the presence of this protein in both the untreated and 4HNE-treated elution lanes, albeit with notably reduced expression in the eluates of 4HNE-exposed GC-2 cells. Taken together with our observations of BAG6 re-localization, these data suggest that oxidative stress induced by 4HNE treatment may result in the disassociation of BAG6 and HSPA2, an event that may influence the susceptibility of HSPA2 to ubiquitination and degradation by the proteasome.

Examination of the relationship between HSPA2, ubiquitin and 4HNE in the spermatozoa of infertile patients

In previous studies we have established that the spermatozoa of infertile men with zona pellucida binding defects are deficient in both HSPA2 (Redgrove et al., 2012) and BAG6 (Bromfield et al., 2015a). To examine the applicability of the current study to these infertile patients we subjected sperm lysates from the same fertile and infertile men to immunoblotting analyses for HSPA2, ubiquitin and 4HNE. Interestingly, spermatozoa from fertile men that have normal expression levels of HSPA2 (as shown in Figure 7A) appeared to possess a number of ubiquitin (Figure 7B) and 4HNE (Figure 7C) adducts with distinct bands present at 72 kDa. This may imply that HSPA2 in the spermatozoa of healthy donors may still be susceptible to the adduction/ubiquitination process during development. However, spermatozoa from infertile patients that have a deficiency in HSPA2, lacked the 72 kDa 4HNE and ubiquitin bands present in the spermatozoa of their fertile counterparts (Figure 7A-C). If a similar oxidative mechanism for HSPA2 degradation occurs in the human testis as

454 described herein for the mouse, we would expect that the loss of HSPA2 via proteolysis would result
455 in the concomitant loss of detectable 4HNE and ubiquitin expression at that molecular weight.
456 Therefore, it is possible that the loss of HSPA2 in male infertility patients may occur through a similar
457 ubiquitin-dependent proteolysis. While this hypothesis requires more rigorous examination with a
458 larger cohort of patients, certainly these data provide support for the use of mouse GC-2 cells as a
459 model for the study of HSPA2 deficiency in male germ cells.

460

461 **DISCUSSION**

462 Reactive aldehyde-induced protein modifications underpin numerous models of cellular dysfunction
463 and degeneration (Bradley et al., 2010; Citron et al., 2016; Kapphahn et al., 2006; Lord et al., 2015).
464 Despite their rapid turnover in the testis, developing spermatozoa are not spared the deleterious
465 consequences of lipid aldehydes, such as 4HNE, and possess many protein and nucleic acid-based
466 targets for adduction (Baker et al., 2015; Aitken et al., 2012). Previously, we have confirmed the
467 targeting of HSPA2 by 4HNE in mature human spermatozoa and linked this aldehyde to a causal role
468 in the dysregulation of zona pellucida-receptor complex assembly and the subsequent loss of sperm-
469 egg interaction *in vitro* (Bromfield et al., 2015a). This work led us to hypothesize that HSPA2
470 deficiency in the infertile population may be underpinned by 4HNE-mediated protein damage
471 occurring during the formation of the mature gametes in the testis. This inclination is supported by
472 previous studies establishing the vulnerability of HSPA2 to rapid degradation by the ubiquitin-
473 proteasome system in the absence of its protective chaperone BAG6 in mouse germ cells (Sasaki et
474 al., 2008). Moreover, it is known that 4HNE and other lipid aldehydes can render their protein
475 substrates more susceptible to degradation (Carbone et al., 2004b; Marques et al., 2004; Botzen and
476 Grune, 2007; Whittsett et al., 2007). The study described in this manuscript proposes a marriage of
477 these events whereby oxidative stress promotes the targeting of HSPA2 by 4HNE, leading to its
478 dissociation from BAG6 and the ensuing degradation of HSPA2 by the ubiquitin-proteasome system

(summarized in Figure 8). To our knowledge, this is the first study to investigate the fate of a 4HNE-modified substrate in developing germ cells.

A key aim of this study was to validate the use of the GC-2 cell line for the study of HSPA2 protein dynamics under conditions of oxidative stress. In comparing the sensitivity of spermatocytes, spermatids and GC-2 cells to oxidative stress, a unique maturation-dependent disparity was encountered whereby HSPA2 protein expression was relatively stable in PS compared to RS. This incongruence may reflect a number of biological differences between spermatocytes and post-meiotic spermatids including differences in proteasome activity (Wojtczak and Kwiatkowska, 2008), detoxification (Den Boer et al., 1990; Nixon et al., 2014), and/or the rate of protein synthesis within the two cell types (Messina et al., 2010). In support of differences in the rate of proteasome activity our pilot data has revealed a 4-fold increase in proteasome activity in spermatids compared to spermatocytes (Supplementary Figure 2C). This enhanced activity may reflect the need for degradation of unnecessary protein content (e.g. histones) as spermatids commence elongation to produce morphologically mature spermatozoa and begin their histone to protamine transition (Kwiatkowska et al., 2003; Wojtczak and Kwiatkowska, 2008). Additionally, examination of the profile of 4HNE-adducted proteins in both round spermatids and pachytene spermatocytes revealed a greater number of 4HNE adducted proteins in the lysate of RS versus PS (Supplementary Figure 2D) suggesting an innate vulnerability to this form of post-translational non-enzymatic modification in spermatids. This may reflect an important change in the lipid composition of developing spermatids as their membranes become enriched with glycerophospholipids and 2-hydroxylated very long chain polyunsaturated fatty acids (Oresti et al., 2010). One may speculate that such developmental changes could lead to an increased yield of 4HNE and other lipid peroxidation products in RS upon oxidative attack.

In a physiological sense, the retention of HSPA2 in PS may be indicative of protective mechanisms in place to ensure HSPA2 can fulfil its role in synaptonemal complex assembly during meiosis (Dix et al., 1996; 1997). Such a role is known to be essential, at least in the mouse, as *Hspa2* -/- mice do not produce post-meiotic germ cells (Dix et al., 1996 a,b). However, the susceptibility of

RS to HSPA2 degradation is particularly interesting as human studies suggest that HSPA2 is expressed at higher levels in elongating spermatids than in spermatocytes (Huszar et al., 2000; Motiei et al., 2013). Accordingly, HSPA2 appears to play an important role in spermiogenesis and has been used as a biomarker of both sperm maturity and IVF success (Ergur et al., 2002; Cayli et al., 2003). Moreover, immature human sperm that fail to express HSPA2 have increased cytoplasmic retention and lack the ability to interact with zona pellucida (Huszar et al., 2000). This effect on zona pellucida interaction mirrors what we have recorded when modelling the effect of 4HNE adduction to HSPA2 in mature spermatozoa *in vitro* (Bromfield et al., 2015b). With these maturational differences in mind, GC-2 cells appear to respond to 4HNE exposure in a manner most similar to RS in terms of HSPA2 stability. This is particularly interesting as the GC-2 cells were originally derived from spermatocytes. However, despite their proliferative nature, GC-2 cells have been reported to display a number of spermatid-like features (Hofmann et al., 1994; Sanborn et al., 1997; Meinhardt et al., 1997). As this cell line also proved more resilient to 4HNE exposure and is known to be appropriate for transfection experiments, these cells were deemed an appropriate model to further investigate the mechanisms behind HSPA2 loss in developing germ cells.

Through both co-migration and immunoprecipitation approaches, we have provided evidence for the ubiquitination of HSPA2 in response to 4HNE exposure in GC-2 cells. As an important precedent for these findings, it has previously been shown that preferential ubiquitination occurs on 4HNE-modified substrates in other cell types such as cultured lens epithelial cells (Marques et al., 2004). Furthermore, chaperones such as alphaB-crystallin that are expressed in these cells are known to be ubiquitinated at a faster rate when modified by 4HNE than in their native form (Marques et al., 2004). With regard to HSPA2, mutational analyses have identified several lysine residues within the protein's primary structure as targets for poly-ubiquitination. Importantly, such residues are conserved between the mouse and human HSPA2 homologues (Sasaki et al., 2008). While the ubiquitin-proteasome system (UPS) affords a logical pathway for the selective degradation of damaged proteins (Sutovsky, 2003), oxidatively-modified proteins are more often degraded by the 20S proteasome in a manner independent of ubiquitin (Shringarpure et al., 2003; Jung and Grune, 2008). This may be due

to oxidative side chain modification occurring at lysine residues that are also the binding sites for ubiquitin (Grune et al., 2003). Although 4HNE modification at lysine residues could also hinder ubiquitin from contacting its substrates, 4HNE preferentially reacts with cysteine residues (Wakita et al., 2009) and accordingly, its known target on HSPA2 is a cysteine that lies within the ATPase domain of the protein (Carbone et al., 2004). While we are yet to confirm whether this cysteine is indeed the target of 4HNE modification in our germ-cell model system, the involvement of the UPS in the degradation of this protein does provide us with a rationale to investigate cysteine- and histidine-based 4HNE modifications on HSPA2 in future experiments.

Using the canonical proteasome inhibitor MG132 as well as the lysosome inhibitor chloroquine we can conclude from the current study that a proteasome-dependent degradation pathway is likely to be involved in the processing of 4HNE-modified HSPA2 in GC-2 cells. This is congruent with studies by Sasaki and colleagues evaluating the loss of HSPA2 in BAG6 -/- mice (Sasaki et al., 2008) and analogous of the processing of other 4HNE modified-proteins such as adiponectin (Wang et al., 2012) and alcohol dehydrogenase (Carbone et al., 2004). The targeted degradation of such proteins is thought to be due to a conformational change induced by the docking of 4HNE leading to the recognition and processing of the oxidized or damaged protein by the UPS. Notwithstanding these data, in other cell types a lysosomal pathway appears to be favoured for the degradation of 4HNE-modified substrates (Marques et al., 2004). While this variation may be due, in part, to the differing cell-types studied, the extent of 4HNE exposure can greatly augment the response mounted by cells (Hohn et al., 2013). Key examples of this exist through studies evaluating 4HNE-induced protein aggregation where moderately modified 4HNE-substrates can be cleared by the proteasome system, while extensively modified substrates often endure extensive crosslinking and become poor substrates for degradation (Okada et al., 1999; Grune and Davies, 2003). Additionally, such cross-linked proteins can be inhibitory to proteasomal degradation pathways and further impair protein turnover within cells (Farout et al., 2006; Friguet et al., 1994; Shringarpure et al., 2000). It is this induction of protein aggregation that implicates 4HNE in cellular degeneration and ageing-related disorders (Shringapure et al., 2000; Hohn et al., 2013).

In the current study, monitoring the chymotrypsin-like activity of the proteasome in GC-2 cell lysates revealed the stimulation of proteasome activity in cells exposed to a moderate concentration of 4HNE. This is interesting as 4HNE itself has been implicated in both proteasomal regulation (Farout et al., 2006) and stimulation (Grune et al., 1995) in independent studies. Nevertheless, it has also been reported that the trypsin and peptidylglutamyl peptide hydrolase activities of the proteasome were transiently diminished in the kidney in accordance with the accumulation of 4HNE-modified proteins (Okada et al., 1999). This loss of proteasome activity may be due to the direct attachment of 4HNE to proteasomal subunits (Okada et al., 1999) and accordingly, a 4HNE modification on the 20S proteasome subunit α7 has been recently identified that may be involved in its regulation in response to oxidative stress (Just et al., 2015). While we have yet to explore the effect of high amounts of 4HNE, such a study could provide great insight into the accumulation of 4HNE-modified substrates in early germ cells and the effect of such deleterious events on cellular apoptosis. Furthermore, evaluating whether increased 4HNE exposure in GC-2 cells can result in either protein-crosslinking and/or a preferential use of a lysosomal degradation pathway would provide further insight into the fate of 4HNE-modified substrates in the testis.

The modification of molecular chaperones by 4HNE has been documented in a number of studies and extends to the HSP70 (Carbone et al., 2004; Baker et al., 2015; Bromfield et al., 2015b) and HSP90 (Carbone et al., 2005) families of chaperones, as well as alphaB-crystallin (Marques et al., 2004). Despite this, the subsequent degradation of these chaperones has not been frequently reported (Marques et al., 2004). This may be due to the important regulatory roles of other co-chaperones and co-factors that ensure the correct function of indispensable cellular chaperones (Mayer and Bukau, 2005; Duncan et al., 2015). Additionally, in many cell systems a high level of redundancy exists such that other members of the chaperone families can play compensatory roles to maintain cellular proteostasis (Duncan et al., 2015). In the case of HSPA2, BAG6 commonly assumes the role of its regulatory chaperone in the testis and is critical for its stabilization (Sasaki et al., 2008). In this light, the dissociation of BAG6 from HSPA2 observed in this study may underpin the sensitivity of HSPA2 to degradation in response to oxidative insult. It remains to be seen whether this dissociation is caused

by a modification to the substrate-binding domain of HSPA2 leading to poor BAG6 recognition or alternatively, whether BAG6 function is modulated by 4HNE, rendering it unable to regulate the stability of HSPA2. Certainly, there is evidence to support the co-dependent nature of these two chaperones in mammalian cells (Corduan et al., 2009; Thress et al., 2001) and thus strategies to co-express and purify this protein complex for study *in vitro* would allow for a better understanding of its response to oxidative stress. As BAG6 and HSPA2 also form a stable complex in human testicular germ cells (Bromfield et al., 2015a), and mature spermatozoa from patients lacking HSPA2 have also been shown to be deficient in BAG6, understanding the dynamics of this complex may prove essential to understanding the underlying cause of poor sperm-egg recognition in our own species.

Finally, to evaluate the applicability of this study to the human patient population, the presence of 4HNE and ubiquitin was assessed in patient samples that were known to be deficient in HSPA2 expression (Bromfield et al., 2015a). In doing so, a distinct lack of 4HNE and ubiquitin adducts at ~72kDa were revealed, a result that reflects our analysis of GC-2 cells lacking HSPA2 following 4HNE exposure. While this does not directly affirm the involvement of 4HNE adduction in the degradation of HSPA2 in human germ cells, it does suggest that, in an absence of patient material, the mouse GC-2 cells deliver an appropriate model for evaluating the mechanisms that underpin idiopathic infertility.

Thus in reconciling these data we propose that oxidative stress occurring in the developing germ cells of the testis promotes the modification of HSPA2 by 4HNE and its subsequent ablation from the developing germ line. A direct consequence of this oxidative pathway is the production of mature spermatozoa with reduced ability to engage in zona pellucida binding (Figure 8). Thus, these data add credence to the development of targeted, lipid-based antioxidant approaches that focus on ameliorating the unregulated production of lipid aldehydes in the testis as a way of improving the state of male reproductive health.

Acknowledgements

The authors acknowledge the contributions of Natalie Trigg, Amanda Anderson, Simone Stanger, Bettina Mihalas and Dr. Shaun Roman. We are also very grateful to the staff and patients of IVFAustralia for the supply of human sperm for the completion of this study. In particular, we would like to thank Dr Andrew Hedges, A/Prof Peter Illingworth, A/Prof Gavin Sacks, and Katherine Nixon.

Authors' roles

E.G.B. conducted the experiments and generated the manuscript. R.J.A. contributed to study design and data interpretation. E.A.M contributed to data interpretation and manuscript editing. B.N. contributed to study design, data interpretation, and manuscript preparation and editing.

Funding

This work was funded by a Project Grant from the National Health and Medical Research Council of Australia (grant number: APP1101953).

Conflict of interest

None declared.

REFERENCES

Aitken RJ. The capacitation-apoptosis highway: oxysterols and mammalian sperm function. *Biol Reprod* 2011;**85**:9–12.

637 Aitken RJ, Irvine DS, Wu FC. Prospective analysis of sperm –oocyte fusion and reactive oxygen
638 species generation as criteria for the diagnosis of infertility. *Am J Obstet Gynecol* 1991;**164**:542–551.

639 Aitken RJ, Whiting S, De Iuliis GN, McClymont S, Mitchell LA and Baker MA. Electrophilic
640 Aldehydes Generated by Sperm Metabolism Activate Mitochondrial Reactive Oxygen Species
641 Generation and Apoptosis by Targeting Succinate Dehydrogenase. *J Biol Chem.* 2012; **287**: 33048-
642 33060.

643 Baker MA, Weinberg A, Hetherington L, Villaverde AI, Velkov T, Baell J, Gordon C. Defining the
644 mechanisms by which the reactive oxygen species by-product, 4-hydroxynonenal, affects human
645 sperm cell function. *Biol Reprod* 2015;**92**:108.

646 Baleato RM, Aitken RJ, Roman SD. Vitamin A regulation of BMP4 expression in the male germ line.
647 *Dev Biol.* 2005; **286**: 78–90.

648 Botzen D, Grune T. Degradation of HNE-modified proteins-possible role of ubiquitin. *Redox Rep*.
649 2007; **12**: 63-67.

650 Bradley MA, Markesbery WR, and Lovell MA. Increased levels of 4-hydroxynonenal and acrolein in
651 the brain in preclinical Alzheimer disease. *Free Rad Biol Med.* 2010; **48**: 1570-1576.
652

653 Bromfield EG, Aitken RJ, Anderson AL, McLaughlin EA, Nixon B. The impact of oxidative stress on
654 chaperone-mediated human sperm-egg interaction. *Hum Reprod.* 2015a; **30**: 2597-2613.

655 Bromfield EG, Aitken RJ, Nixon B. Novel characterization of the HSPA2-stabilizing protein BAG6
656 in human spermatozoa. *Mol Hum Reprod.* 2015b; **21**: 755-769.

657 Bromfield EG, McLaughlin EA, Aitken RJ, Nixon B. Heat Shock Protein member A2 forms a stable
658 complex with angiotensin converting enzyme and protein disulphide isomerase A6 in human
659 spermatozoa. *Mol Hum Reprod.* 2016; **22**: 93-109.

660 Butterfield DA. Amyloid beta-peptide (1–42)-induced oxidative stress and neurotoxicity: implications
661 for neurodegeneration in Alzheimer's disease brain: a review. *Free Radic Res.* 2002;**36**:1307–1313.

662 Carbone DL, Doorn JA, Petersen DR. 4-Hydroxynonenal regulates 26S proteasomal degradation of
663 alcohol dehydrogenase. *Free Radic Biol Med.* 2004;**37**:1430-1439.

664 Cheetham ME, Chapple JP and can der Spuy J. In: The Networking of Chaperones by co-chaperones:
665 (2015). *Subcellular Biochemistry* **78**. Springer International Publishing, Switzerland.

666 Chondrogianni N, Petropoulos I, Grimm S, Georgilla K, Catalgol B, Friguet B, Grune T, Gonos ES.
667 Protein damage, repair and proteolysis. *Mol Asp. Med.* 2014; **35**: 1-71.

668 Citron BA, Ameenuddin S, Uchida K, Suo WZ, SantaCruz K, and Festoff BW. Membrane lipid
669 peroxidation in neurodegeneration: Role of thrombin and proteinase-activated receptor-1. *Brain*
670 *Res*. 2016; **1643**: 10-17.

671 Corduan A, Lecomte S, Martin C, Michel D, Desmots F. Sequential interplay
672 between BAG6 and HSP70 upon heat shock. *Cell Mol Life Sci.* 2009; **66**:1998-2004.

673 Den Boer PJ, Poot M, Verkerk A, Jansen R, Mackenbach P, Grootegoed JA. Glutathione-dependent
674 defence mechanisms in isolated round spermatids from the rat. *Int J Androl.* 1990; **13**: 26-38.

675 Dix DJ, Allen JW, Collins BW, Mori C, Nakamura N, Poorman-Allen P, Goulding EH and Eddy EM.
676 Targeted gene disruption of Hsp70-2 results in failed meiosis, germ cell apoptosis, and male infertility
677 *Proc Nat Acad Sci USA.* 1996; **93**: 3264–3268.

678 Dunmore BJ, Drake KM, Upton PD, Toshner MR, Aldred MA, Morrell NW. The lysosomal inhibitor,
679 chloroquine, increases cell surface BMPR-II levels and restores BMP9 signalling in endothelial cells
680 harbouring BMPR-II mutations. *Hum Mol Genet.*2013; **22**: 3667-3679.

681 Eddy EM. Role of heat shock protein HSP70-2 in spermatogenesis. *Rev Reprod.* 1999; **1**: 23-30.

682 Ergur AR, Dokras A, Giraldo JL, Habana A, Kovanci E, Huszar G. Sperm maturity and treatment
683 choice of in vitro fertilization (IVF) or intracytoplasmic sperm injection: diminished sperm HspA2
684 chaperone levels predict IVF failure. *Fertil Steril.* 2002;**77**:910– 918.

685 Esterbauer H, Schaur RJ, Zollner H. Chemistry and biochemistry of 4-hydroxynonenal,
686 malonaldehyde and related aldehydes. *Free Radic Biol Med*. 1991; **11**: 81–128.

687 Farout L, Mary J, Vinh J, Szweda LI, Friguet B. Inactivation of the proteasome by 4-hydroxy-2-
688 nonenal is site specific and dependant on 20s proteasome subtypes. *Arch. Biochem. Biophys.* 2006;
689 **453**: 135–142.

690 Forman HJ. Reactive oxygen species and α,β-unsaturated aldehydes as second messengers in signal
691 transduction. *Ann N Y Acad Sci*. 2010; **1203**: 35-44.

692 Friguet B, Szweda LI, Stadtman ER. Susceptibility of glucose-6-phosphate dehydrogenase modified
693 by 4-hydroxy-2-nonenal and metal-catalyzed oxidation to proteolysis by the multicatalytic protease.
694 *Arch. Biochem. Biophys.* 1994; **311**: 168-173.

695 Grune T, Reinheckel T, Joshi M, Davies KJA. Proteolysis in cultured liver epithelial cells during
696 oxidative stress. *J. Biol. Chem.* 1995; **270**: 2344–2351

697 Grune T, Davies KJ. The proteasomal system and HNE-modified proteins. Mol Aspects Med. 2003a;
698 24: 195-204.

699

700 Grune T, Merkera K, Sandiga G, Davies KJA. Selective degradation of oxidatively modified protein
701 substrates by the proteasome. *Biochem Biophys Res Commun.* 2003b; **305**: 709-718.

702 Höhn A, König J, Grune T. Protein oxidation in aging and the removal of oxidized proteins. *J Prot*.
703 2013; **92**: 132-159.

704 Huszar G, Ozkavukcu S, Jakab A, Celik-Ozenci C, Sati GL, Cayli S. Hyaluronic acid binding ability
705 of human sperm reflects cellular maturity and fertilizing potential: selection of sperm for
706 intracytoplasmic sperm injection. *Curr Opin Obstet Gynecol* 2006;**18**:260–267.

707 Iwasaki A, Gagnon C. Formation of reactive oxygen species in spermatozoa of infertile patients.
708 *Fertil Steril* 1992; **57**: 409-16.

709 Jones R, Mann T and Sherins R. Peroxidative breakdown of phospholipids in human spermatozoa,
710 spermicidal properties of fatty acid peroxides, and protective action of seminal plasma. *Fertil Steril*.
711 1991;**31**: 531-537.

712 Jung T, Grune T. The Proteasome and its role in the degradation of oxidized proteins. *IUBMB Life*.
713 2008; **60**: 743-752.

714 Just J, Jung T, Friis NA, Lykkemark S, Drasbek K, Siboska G, Grune T, Kristensen P. Identification
715 of an unstable 4-hydroxynonenal modification on the 20S proteasome subunit α7 by recombinant
716 antibody technology. *Free Radic Biol Mol*. 2015; **89**: 786-792.
717

718 Kapphahn RJ, Giwa BM, Berg KM, Roehrich H, Feng X, Olsen TW, Ferrington DA. Retinal proteins
719 modified by 4-hydroxynonenal: identification of molecular targets. *Exp Eye Res*. 2006; **83**: 165-175.
720

721 Katen AL, Chambers CG, Nixon B, Roman SD. Chronic acrylamide exposure in male mice results in
722 elevated DNA damage in the germline and heritable induction of CYP2E1 in the testes. *Biol Reprod*.
723 2016; pii: biolreprod.116.139535.
724

725 Koh YH, von Arnim CAF, Hyman BT, Tanzi RE, Tesco G. BACE is degraded via the lysosomal
726 pathway. *J Biol Chem*. 2005; **280**: 32499-504.
727

728 Kwiatkowska M, Wojtczak A, Popłońska K, Teodorczyk M. The influence of epoxomicin, inhibitor
729 of proteasomal proteolytic activity, on spermiogenesis in Chara vulgaris. *Folia Histochem*
730 *Cytobiol*. 2003; **41**: 51-54.
731

732 Lord T, Martin JH, and Aitken RJ. Accumulation of Electrophilic Aldehydes During Postovulatory
733 Aging of Mouse Oocytes Causes Reduced Fertility, Oxidative Stress, and Apoptosis. *Biol Reprod*.
734 2015; **92**: 1-13.

735 Mallette FA, Richard S. K48-linked ubiquitination and protein degradation regulate 53BP1
736 recruitment at DNA damage sites. *Cell Res*. 2012; **22**: 1221-1223.

737 Marques C, Pereira P, Taylor A, Liang JN, Reddy VN, Szweda LI, Shang F. Ubiquitin-dependent
738 lysosomal degradation of the HNE-modified proteins in lens epithelial cells. *FASEB J*. 2004; **18**:
739 1424-1426.

740 Mayer MP, Bukau B. Hsp70 chaperones: Cellular functions and molecular mechanism. *Cell Mol Life*
741 *Sci*. 2005; **62**: 670-684.

742 Messina V, Di Sauro A, Pedrotti S, Adesso L, Latina A, Geremia R, Rossi P, Sette C. Differential
743 Contribution of the MTOR and MNK Pathways to the Regulation of mRNA Translation in Meiotic
744 and Postmeiotic Mouse Male Germ Cells. *Biol Reprod.* 2010; **83**: 607-615.

745 Moazamian R, Polhemus A, Connaughton H, Fraser B, Whiting S, Gharagozloo P, Aitken RJ.
746 Oxidative stress and human spermatozoa: diagnostic and functional significance of aldehydes
747 generated as a result of lipid peroxidation. *Mol Hum Reprod.* 2015; **21**: 502-515.

748 Motiei M, Tavalaee M, Rabiei F Hajihosseini R, Nasr-Esfahani MH. Evaluation of HSPA2 in fertile
749 and infertile individuals. *Andrologia*; 2013; **45**:66-72.

750 Nixon B, Bromfield EG, Dun MD, Redgrove KA, McLaughlin EA, Aitken RJ. The role of the
751 molecular chaperone heat shock protein A2 (HSPA2) in human sperm-egg recognition. *Asian J*
752 *Androl* 2015;**17**:568 – 573.

753 Nixon BJ, Katen AL, Stanger SJ, Schjenken JE, Nixon B, Roman SD. Mouse Spermatocytes Express
754 CYP2E1 and Respond to Acrylamide Exposure. *PLoS One*. 2014; **9**: e94904.

755 Okada K, Wangpoengtrakul C, Osawa T, Toyokuni S, Tanaka K, Uchida K. 4-Hydroxy-2-nonenal-
756 mediated impairment of intracellular proteolysis during oxidative stress. *J. Biol. Chem*. 1999; **274**:
757 23787–23793.

758

759 Oresti GM, Reyes JG, Luquez JM, Osses N, Furland NE, Aveldaño MI. Differentiation-related
760 changes in lipid classes with long-chain and very long-chain polyenoic fatty acids in rat
761 spermatogenic cells. *FASEB J*. 2004; **18**: 1424-1426.
762
763 Perluigi M, Coccia R, Butterfield DA. 4-hydroxy-2-nonenal, a reactive product of lipid peroxidation,
764 and neurodegenerative diseases: a toxic combination illuminated by redox proteomics studies.
765 *Antioxid Redox Signal* 2012;**17**:1590 – 1609.

766 Rao B, Soufir JC, Martin M, David G. Lipid peroxidation in human spermatozoa as related to
767 midpiece abnormalities and motility. *Gamete Res* 1989;**24**:127–134.

768 Redgrove KA, Nixon B, Baker MA, Hetherington L, Baker G, Liu DY, Aitken RJ. The molecular
769 chaperone HSPA2 plays a key role in regulating the expression of sperm surface receptors that
770 mediate sperm–egg recognition. *PLoS One* 2012;**7**:e50851.

771 Redgrove KA, Anderson AL, McLaughlin EA, O'Bryan MK, Aitken RJ, Nixon B. Investigation of
772 the mechanisms by which the molecular chaperone HSPA2 regulates the expression of sperm surface
773 receptors involved in human sperm–oocyte recognition. *Mol Hum Reprod* 2013;**19**:120 – 135.

774 Reid AT, Lord T, Stanger SJ, Roman SD, McCluskey A, Robinson PJ, Aitken RJ, Nixon B. Dynamin
775 regulates specific membrane fusion events necessary for acrosomal exocytosis in mouse spermatozoa.
776 *J Biol Chem* 2012; **287**:37659– 37672.

777 Sasaki T, Marcon E, McQuire T, Arai Y, Moens PB, Okada H. Bat3 deficiency accelerates the
778 degradation of Hsp70–2/HspA2 during spermatogenesis. *J Cell Biol* 2008;**182**:449–458.

779 Scieglinska D, Krawczyk Z. Expression, function, and regulation of the testis enrichedheat shock
780 HSPA2 gene in rodents and humans. *Cell Stress Chaperones*. 2015; **20**: 221-235.

781 Shang F, Nowell TR, Taylor A. Removal of oxidatively damaged proteins from the lens by the
782 ubiquitin-proteasome pathway. *Exp. Eye. Res*. 2001; **73**: 229-238.

783 Shringarpure R, Grune T, Sitte N, Davies KJA. 4-Hydroxynonenal-modified amyloid-*β* peptide
784 inhibits the proteasome: possible importance for Alzheimer's disease. *Cell. Mol. Life Sci.* 2000; **57**:
785 1802–1809
786 Shringarpure R, Grune T, Mehlhase J, Davies KJ. Ubiquitin conjugation is not required for the
787 degradation of oxidized proteins by proteasome. *J. Biol. Chem*. 2005; **278**: 311–318.

788 Sutovsky P. Ubiquitin-dependent proteolysis in mammalian spermatogenesis, fertilization, and sperm
789 quality control: killing three birds with one stone. *Microsc Res Tech.* 2003; **61**:88-102.

790 Thress, K., Song, J., Morimoto, R. I. and Kornbluth, S. Reversible inhibition of Hsp70 chaperone
791 function by Scythe and Reaper. *EMBO J*. 2001; **20**, 1033 – 1041.

792 Towbin H, Staehelin T, Gordon J. Electrophoretic transfer of proteins from polyacrylamide gels to
793 nitrocellulose sheets: procedure and some applications. *Biotechnology*. 1979;**24**:145– 149.

794 Tremellen K. Oxidative stress and male infertility: a clinical perspective. *Hum Reprod Update* 2008;
795 **14**: 243-58.

796 Uchida K, Stadtman ER. Covalent attachment of 4-hydroxynonenal to glyceraldehyde-3-phosphate
797 dehydrogenase. A possible involvement of intra- and intermolecular cross-linking reaction. *J Biol*
798 *Chem*. 1993; **268**: 6388-93.

799 Uchida K. 4-Hydroxy-2-nonenal: a product and mediator of oxidative stress. *Prog Lipid Res*
800 2003;**42**:318–343.

801 Wakita C, Maeshima T, Yamazaki A, Shibata T, Ito S, Akagawa M, Ojika M, Yodoi J, Uchida K.
802 Stereochemical configuration of 4-hydroxy-2-nonenal-cysteine adducts and their stereoselective
803 formation in a redox-regulated protein. *J Biol Chem*. 2009; **284**: 28810-28822.

804 Wang Z, Dou X, Gu D, Shen C, Yao T, Nguyen V, Braunschweig C, Song Z. 4-Hydroxynonenal
805 differentially regulates adiponectin gene expression and secretion via activating PPARγ and
806 accelerating ubiquitin-proteasome degradation. *Mol Cell Endocrinol*. 2012; **349**: 222-231.

Whitsett J, Picklo MJ Sr, Vasquez-Vivar J. 4-Hydroxy-2-nonenal increases superoxide anion radical in endothelial cells via stimulated GTP cyclohydrolase proteasomal degradation. *Arterioscler Thromb Vasc Biol.* 2007; **27**: 2340-2347.

Wojtczak A, Kwiatkowska M. Immunocytochemical and Ultrastructural Analyses of the Function of the Ubiquitin Proteasome System During Spermiogenesis with the Use of the Inhibitors of Proteasome Proteolytic Activity in the Alga, Chara vulgaris. *Biol Reprod*. 2008; **78**: 577-585.

FIGURE LEGENDS

Figure 1: Heat shock protein A2 (HSPA2) protein levels in response to oxidative stress in isolated mouse germ cells.

(A) Pachytene spermatocytes, (B) round spermatids and (C) GC-2 cells were treated with 4-hydroxynonenal (4HNE) to induce oxidative stress and lysed alongside their untreated (UT) counterparts. Protein lysates were subjected to sodium dodecyl sulphate - polyacrylamide gel electrophoresis (SDS-PAGE) and transferred to nitrocellulose membranes for immunoblotting with anti-HSPA2 antibodies. Immunoblots were probed with anti-HSPA2 antibodies then stripped and re-probed with anti-tubulin antibodies. HSPA2 protein levels were quantified relative to tubulin via band densitometry analysis. Three replicate blots were used in the calculation of band density. Data are presented as mean ± SEM, ** $P < 0.01$, *** $P < 0.001$ versus UT (using a two-tailed, unpaired Student's t test, and in all other figures).

Figure 2: Immunolocalization of HSPA2 and ubiquitin in mouse germ cells exposed to 4HNE. (A) Pachytene spermatocytes, (B) round spermatids and (C) GC-2 cells were treated with 4HNE and

fixed for immunocytochemistry with anti-HSPA2 (green) and anti-UBI-1 (red) antibodies and counterstained with DAPI (blue). Confocal microscopy images were captured using a 60 × objective (A-C), scale = 10 µm, inserts 5 µm (A & C). (B) Scale = 5 µm, inserts 2.5 µm. Fluorescence intensity of HSPA2 and UBI-1 was quantified for 4HNE treated cells using their UT counterparts for reference in three independent replicate populations. Data are presented as mean ± SEM, ** $P < 0.01$, * $P < 0.05$ versus UT.

Figure 3: 4HNE exposure induces changes in the ubiquitin profile of GC-2 cell lysate.

GC-2 cells were exposed to either 50 µM or 200 µM 4HNE for 3 h and then lysed for immunoblotting experiments. (A) A ubiquitin-lysine-48 (K48)-specific antibody was used to assess degradation-related ubiquitination of germ-cell derived proteins with immunoblotting revealing the presence of a ~ 72 kDa band in GC-2 cells exposed to 50 µM 4HNE. Densitometry was performed on this 72 kDa band (indicated by the arrow) across control and treatment lanes relative to anti-tubulin immunoblots, revealing an increase in the ubiquitin signal at 72 kDa in lanes corresponding to 50 µM 4HNE treatment and a subsequent reduction in ubiquitin signal after 200 µM 4HNE exposure. (B) Corresponding immunoblots were probed with anti-HSPA2 antibodies revealing a decrease in HSPA2 band density relative to tubulin (indicated by the arrow) with increasing concentration of 4HNE. Three replicate blots were analysed for these experiments with data presented as mean ± SEM. ** $P < 0.01$, * $P < 0.05$ versus UT.

Figure 4: Immunoprecipitation reveals the adduction of 4HNE and ubiquitin to HSPA2 under conditions of oxidative stress. Confirmation of HSPA2/4HNE/ubiquitin interaction in hydrogen peroxide (H_2O_2) treated GC-2 cells was sought using an immunoprecipitation strategy in which HSPA2 was used as bait to pull down interacting partners. The captured proteins from UT and 50 µM H_2O_2 treated GC-2 cells were eluted from protein G beads and resolved on SDS-PAGE gels alongside an antibody-only control (Ab control), a bead-only control (Bead control), and a precleared control (preclear). (A) HSPA2 immunoprecipitated blots were probed with anti-HSPA2, and the specificity of the immunoprecipitation was confirmed through the detection of a 72 kDa band in the elution lanes

but importantly, not in the control lanes. Probing these blots with anti-4HNE (B) and anti-UBI-k48 revealed the presence of 4HNE and ubiquitin in the 'H_2O_2' immunoprecipitated eluate at 72 kDa (denoted by the arrowheads) but not in the control lanes. Bands present at ~ 35 kDa in all blots appeared to be indicative of antibody contamination as they aligned with bands from the 'antibody only' control lane. Three replicates immunoprecipitation experiments were performed with replicate immunoblots.

Figure 5: HSPA2 loss from GC-2 cells can be prevented through inhibition of the proteasome. (A) GC-2 cells were treated with 200 µM 4HNE in the presence or absence of the proteasome inhibitor MG132 (10 µM) and then lysed for immunoblotting analysis with anti-HSPA2 antibodies. These analyses revealed that inhibition of the proteasome prevented the degradation of HSPA2 in response to 4HNE. Conversely, inhibition of the lysosomal pathway with 100 µM chloroquine (B) did not prevent the loss of the 72 kDa HSPA2 band. (C) Chymotrypsin-like activity of the proteasome was monitored in untreated and 4HNE-treated GC-2 cells via a fluorometric proteasome activity assay kit. This assay measures proteasome activity using an 7-amino-4-methylcoumarin (AMC)-tagged peptide substrate that releases fluorescent AMC in the presence of proteolytic activity. An internal MG132 control was used in this assay to distinguish proteasome activity from other protease activity in the cell lysates, with one unit of proteasome activity defined as the amount of proteasome that generates 1.0 nmol of AMC per minute at 37˚C. This assay detected a significant increase in proteasome activity in 4HNE-treated GC-2 cells. This experiment was repeated across three independent replicates with data presented as mean ± SEM, * $P < 0.05$ versus UT.

Figure 6: Dissociation of HSPA2 from its stabilising co-chaperone BCL2-associated athanogene 6 (BAG6) occurs in response to oxidative stress in GC-2 cells. (A) Untreated and 4HNE treated GC-2 cell lysates were prepared for immunoblotting with anti-BAG6 antibodies. Band density analysis, performed relative to tubulin, revealed no significant difference between the 120 kDa band corresponding to BAG6 in untreated and 4HNE treated samples. Comparing mean values from three replicates revealed no significant differences between 4HNE treated and UT lanes in terms of BAG6 band density (n=3; $P > 0.05$), data are presented as mean ± SEM. (B) Immunocytochemistry on

untreated and 4HNE treated GC-2 cells with anti-BAG6 antibodies revealed the presence of the protein in GC-2 cells (green) with a re-localization to the periphery of the cell apparent in response to 4HNE. Scale = 5 µm. (C) Proximity ligation of BAG6 and HSPA2 was performed in GC-2 cells. An association of the two proteins was apparent in untreated cells, as indicated by punctate fluorescent foci (red). These cells were counterstained with DAPI (blue) for clarity. An absence of HSPA2/BAG6 association was observed in 4HNE treated cells as evidenced by a lack of red fluorescence. Scale = 5 µm, n = 3 (D) Confirmation of HSPA2/BAG6 dissociation in 4HNE treated GC-2 cells was sought using an immunoprecipitation strategy in which HSPA2 was used as bait to pull down interacting partners. The captured proteins from UT and 50 µM H_2O_2 treated GC-2 cells were eluted from protein G beads and resolved on SDS-PAGE gels alongside an antibody-only control (Ab control), a bead-only control (Bead control), and a precleared control (preclear). (A) HSPA2 immunoprecipitated blots were probed with anti-BAG6 revealing a reduction in the presence of this ~120 kDa protein in 4HNE-treated GC-2 cell eluates. Probing these blots with anti-HSPA2 confirmed the specificity of the immunoprecipitation through the detection of a 72 kDa band in the elution lanes but importantly, not in the control lanes (n=3).

Figure 7: Analysis of 72 kDa 4HNE and ubiquitin adducts in the spermatozoa of infertile men. Infertile male IVF patients were selected based on a complete failure of sperm–zona pellucida binding following standard IVF. The spermatozoa from two patients were subjected to SDS-extraction and lysates were resolved alongside two known fertile sperm lysate controls on SDS gels before being transferred to nitrocellulose membranes for immunoblotting. Probing of these lysates with anti-HSPA2 (A), anti-ubiquitin (B) and anti-4HNE (C) revealed the constitutive adduction of a ~72 kDa protein in the fertile patients but an absence of this adduct in the infertile patients (n=2). Importantly protein loading was revealed by incubating each blot with an anti-tubulin antibody (D)

Figure 8: Oxidative stress in testicular germ cells may lead to HSPA2 proteolysis. Taken together, our data suggest that oxidative stress (1), known to result in the generation of 4HNE via lipid

peroxidation (2-3), can lead to the modification of HSPA2 by 4HNE adduction resulting in its dissociation from its stabilizing-chaperone BAG6 (4). This may in turn expose HSPA2 to ubiquitin ligases leading to its ubiquitination and degradation via a proteasome-dependent mechanism (5). We predict that spermatozoa would then be released from the testis with a deficiency in HSPA2 protein levels (6), which could result in perturbed zona pellucida receptor-complex assembly during capacitation in the female reproductive tract and thus limit the ability of these cells to engage in interactions with the oocyte (7). PS: Pachytene spermatocytes, RS: round spermatids

Supplementary Figure 1: Cell viability after 4HNE and H_2O_2 treatment. (A) PS), RS and GC-2 cells were treated with either 4HNE or H_2O_2 at concentrations ranging from 50 µM to 200 µM for 3 h. Cell viability was scored post-treatment using an Eosin viability stain over three biological replicates. Horizontal lines reflect 50% viability of cell populations. Data are presented as mean ± SEM, n=3 (B) PS were treated with either 50 µM or 200 µM 4HNE and then lysed for use in immunoblotting experiments. Lysates were subjected to SDS-PAGE alongside untreated PS lysate (for comparison) and probed with anti-HSPA2 antibodies to evaluate HSPA2 protein levels. Equivalent protein loading was determined by re-probing immunoblots with anti-tubulin antibodies (n=3). (C) GC-2 cells were treated with either 50 µM or 200 µM hydrogen peroxide and then lysed for use in immunoblotting experiments. Lysates were subjected to SDS-PAGE alongside 200 µM 4HNE-treated GC-2 cell lysate (for comparison) and an untreated control and probed with anti-HSPA2 antibodies to evaluate HSPA2 protein levels. Equivalent protein loading was determined by re-probing immunoblots with anti-tubulin antibodies (n=3).

Supplementary Figure 2: Comparison of proteasome activity and 4HNE adduction in spermatocytes and spermatids. (A) The specificity of the proximity ligation assay conducted to evaluate the association of BAG6 and HSPA2 was verified by the inclusion of an irrelevant antibody control (tubulin/BAG6) that revealed no red fluorescent signal alongside DAPI and phase images. Scale = 5 µM, n=3. (B) Untreated and 4HNE-treated GC-2 cells were separated into their nuclear and cytoplasmic compartments and lysed with NP40 buffer alongside their whole cell counterparts. Efficacy of this fractionation was confirmed through immunoblotting with anti-tubulin and anti-

939 Fibrillarin antibodies to demonstrate an enrichment of cytoplasmic and nuclear components,
940 respectively. Probing of corresponding Western blots with anti-BAG6 revealed a modest reduction in
941 BAG6 protein expression in the nuclear fraction of 4HNE-treated GC-2 cells (n=3). (C)
942 Chymotrypsin-like activity of the proteasome was monitored in pachytene spermatocytes (PS) and
943 round spermatids (RS) via a fluorometric proteasome activity assay kit. This assay measures
944 proteasome activity using anAMC-tagged peptide substrate that releases fluorescent AMC in the
945 presence of proteolytic activity. An internal MG132 control was used in this assay to distinguish
946 proteasome activity from other protease activity in the cell lysates with one unit of proteasome
947 activity defined as the amount of proteasome that generates 1.0 nmol of AMC per minute at 37˚C.
948 This assay detected a significantly higher level of proteasome activity in RS compared to PS (* $P <$
949 0.05; n=3). (D) The 4HNE profile of untreated PS and RS was assessed using an antibody to 4HNE.
950 A greater number of adducts were observed in the RS lysate compared to the PS lysate. Even loading
951 was confirmed by re-probing immunoblots with anti-tubulin antibodies (n=3).

952

Bromfield et al_Figure 1

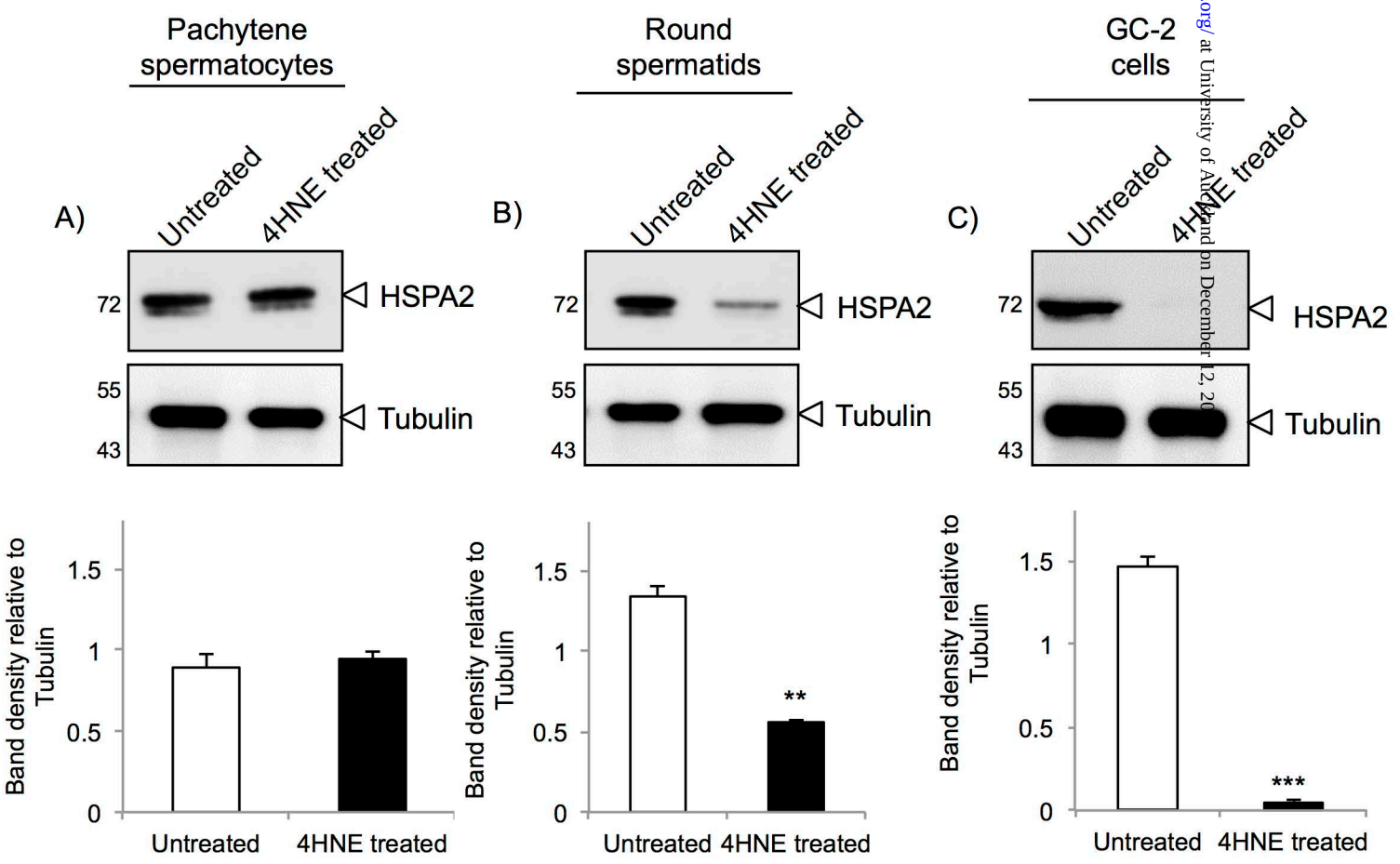

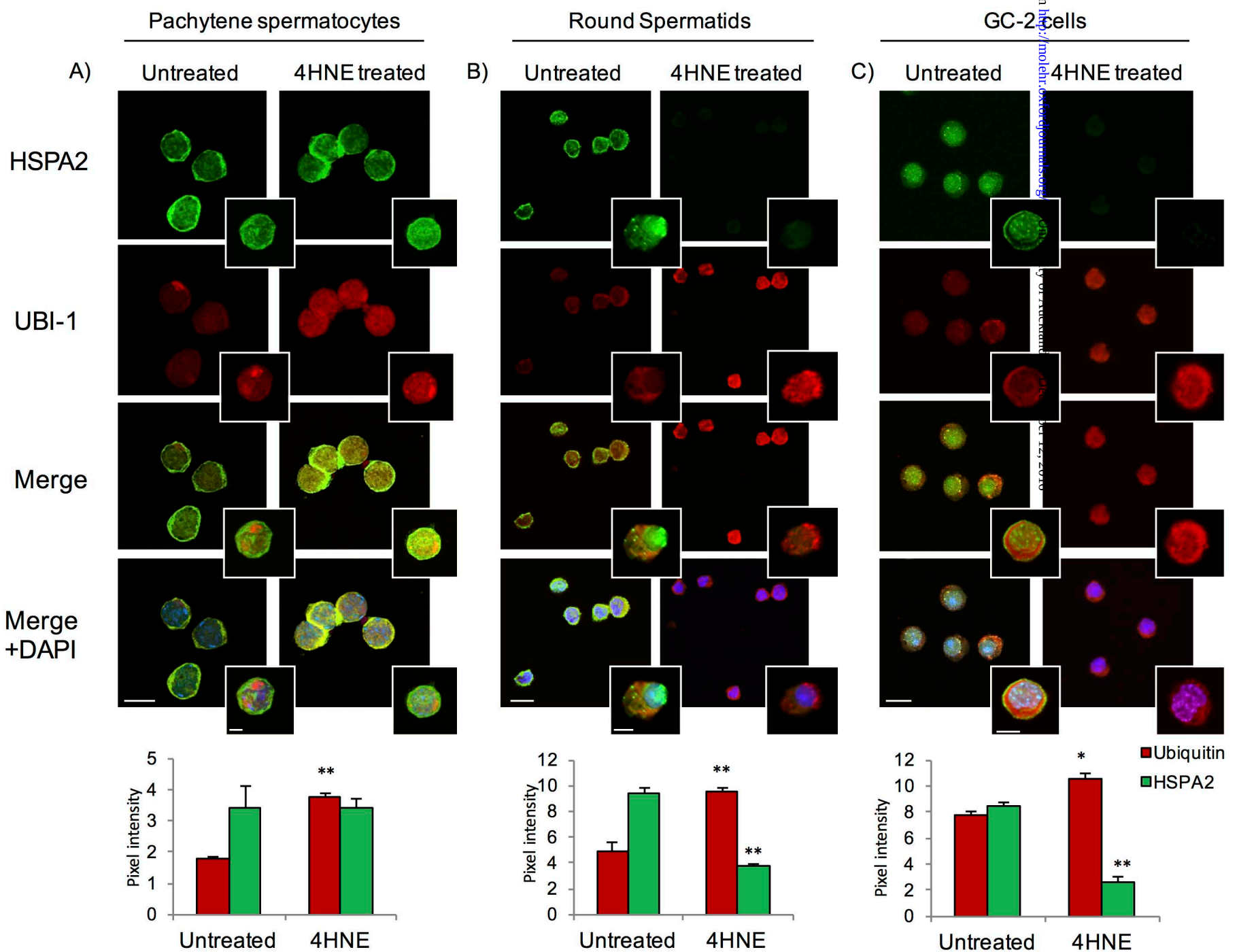

Bromfield et al_Figure 3

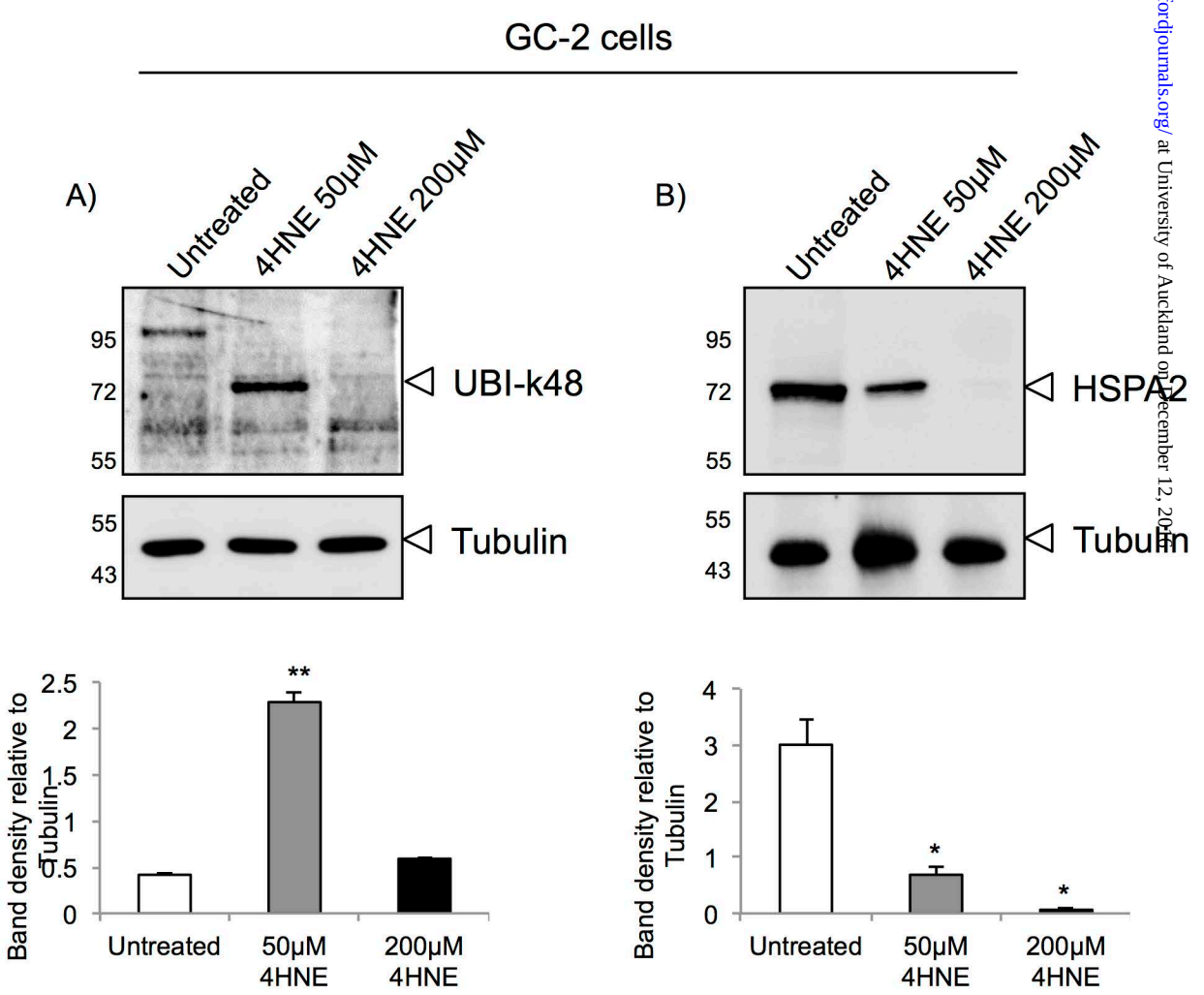

Bromfield et al_Figure 4

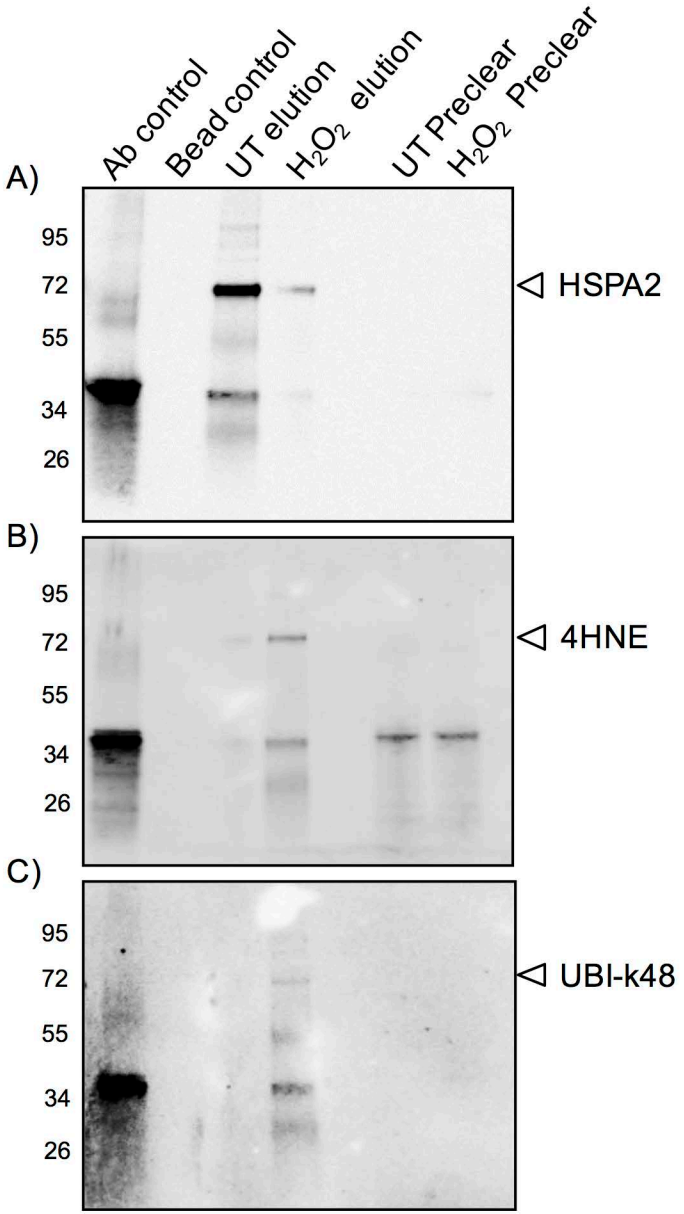

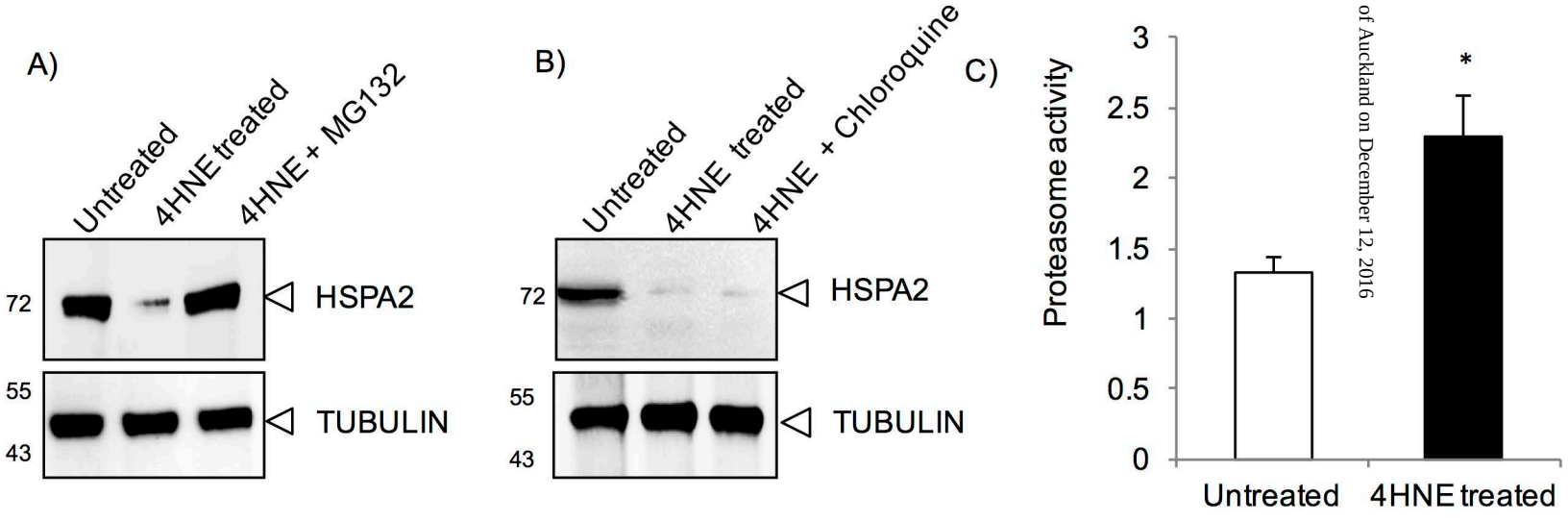

BAG6 expression

A)

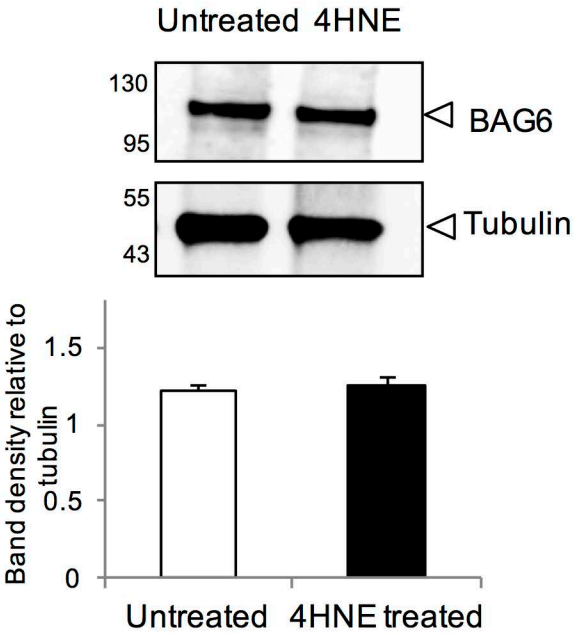

B)

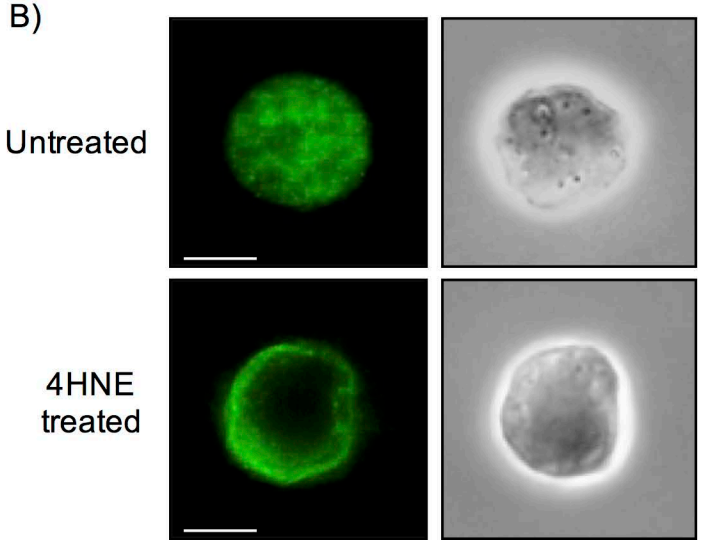

Proximity Ligation Assay

C)

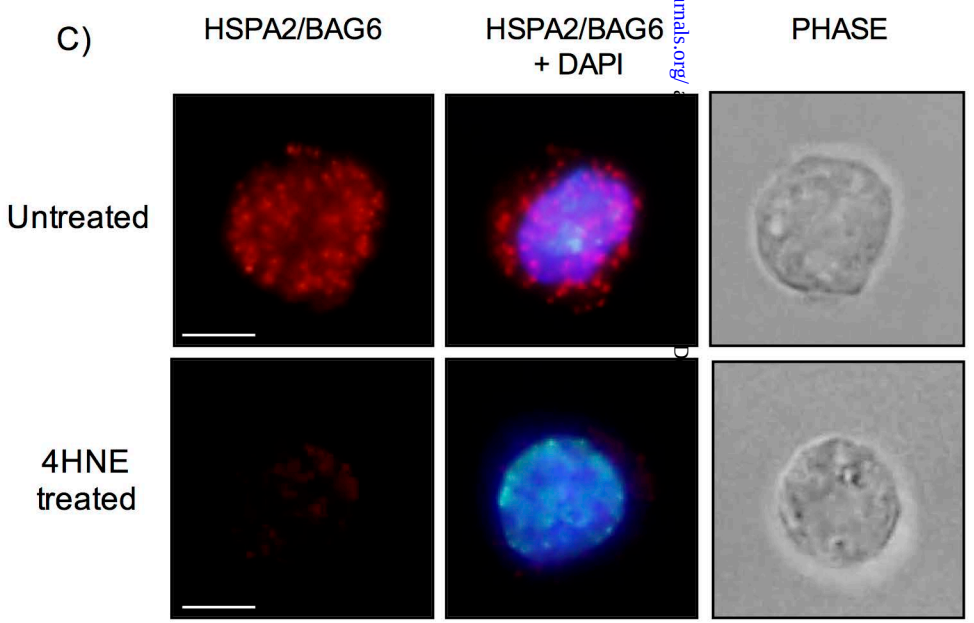

D)

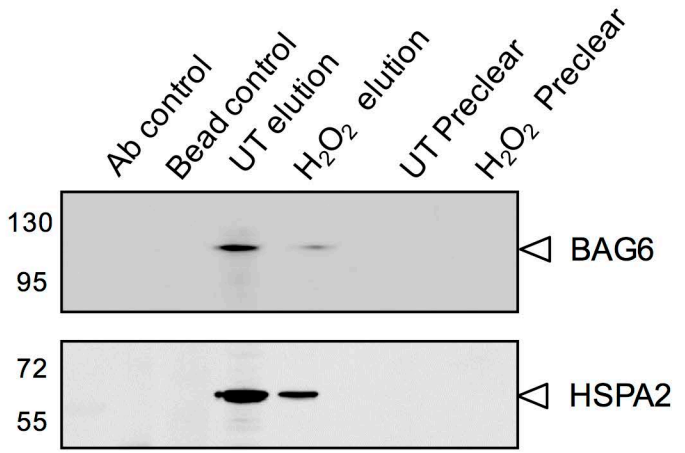

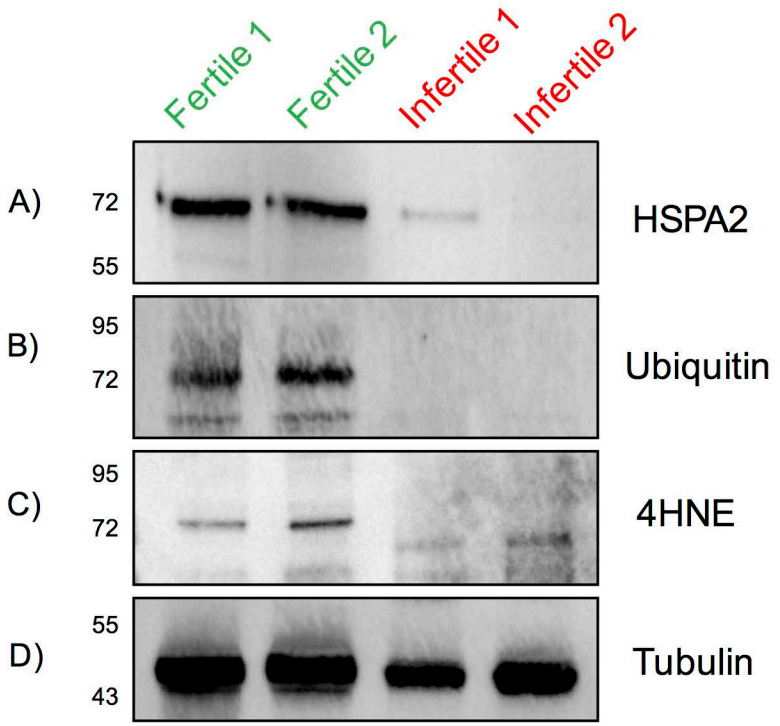

Bromfield et al_Figure 8